Path integral Monte Carlo study of the hydrated electron[a]

A. Wallqvist, D. Thirumalai,[b] and B. J. Berne
Department of Chemistry, Columbia University, New York, New York 10027

(Received 13 November 1986; accepted 20 January 1987)

The structure of an excess electron in water at room temperature is investigated using the Feynman path integral technique. The interaction potential between the electron and water is modeled by an effective potential, made up of three terms: a static potential, a repulsive potential, and a polarization potential. The polarization part is treated in two different ways: approximated as pairwise additive, and exactly with the many body polarization effects treated self-consistently. It is shown that the excess electron forms a cavity with the radius of the electron being 2.24 Å for pairwise additive polarization and 2.11 Å for the self-consistent treatment of the polarization. There is no sharp geometrical coordination number of water molecules around the electron. The water molecules within a distance of about 3.5 Å from the center of the electronic change distribution point their OH bonds towards the electron, and form only three hydrogen bonds. It is also found that the pair correlation function of the solvent molecules close to the electron are considerably different from the corresponding quantities calculated in the bulk. The electron, therefore, is shown to modify the local density to a large extent. There are important structural differences between the many body polarization model and the two body polarization model. It is concluded that for a quantitative description of the structure of the hydrated electron, the self-consistent treatment of the long range (many body) polarization effects are important.

I. INTRODUCTION

The properties of the solvated electron have been extensively studied.[1–3] Despite this there are several facets of the general problem of an excess electron in polar solvents that are not well understood. For example, there is no satisfactory theoretical model that explains either the kinetics of localization of an e^- in polar solvents[4] or the optical absorption spectra.[5] The difficulty in constructing a suitable theory stems from the very rich and varied behavior of excess electrons in polar (as well as nonpolar) fluids.[6] Depending upon the thermodynamic state and the nature of the solvent, the excess electron exhibits varying degrees of localization. One of the major difficulties in investigating the states of an electron in polar solvents is that they depend critically on the electron–solvent interaction and this is not known. Simple model potentials have therefore been constructed to account for the experimental measurements.[2,3] Besides being empirical, such an approach does not provide a complete understanding of electron solvation, because the role of the solvent is not explicitly included. Such treatments cannot deal with the response of the solvent to the presence of the excess electron.[7] In order to overcome some of the difficulties of these earlier approaches we present an alternative, and hopefully, a more general treatment of electron solvation in polar media. The approach essentially involves devising a local pseudopotential to characterize the interaction between the electron and the polar molecule. Assuming that the interaction potential between solvent molecules is known, we use the path integral Monte Carlo technique to investigate the physical properties of the solvated electron.[8] Needless to say the results will depend on the details of the electron–molecule pseudopotential. Since the pseudopotential has been obtained by a more systematic approach than that used in simple model calculations,[2,3] the simulations here should provide a better understanding of the equilibrium properties of the solvated electron.

The most direct probe of the interaction between the electron and the polar solvent is through the use of spectroscopic techniques.[9] Numerous studies of the optical absorption spectrum of the hydrated electron at room temperatures have been reported. All of these studies show that the absorption spectrum is structureless and is asymmetric about the band maximum at 1.73 eV with a high frequency wing.[10] The pressure dependence[11] of the optical absorption spectrum indicates that the band maximum increases from 1.73 to 2.00 eV as the pressure is varied from 1 bar to 6.3 kbar while the full width at half-maximum increases from 0.8 to about 1 eV. Subsequent studies by Hentz *et al.*[12] of the volume of excitation for the reaction of the hydrated electron in water suggested that the cavity size decreases with increasing pressure. This could account for the pressure dependence of the spectroscopic measurements and stands in contrast to the model of Copeland, Kestner, and Jortner[7] who have assumed that the cavity radius is independent of pressure.

[a] This work was supported by a grant from NSF and by a grant of supercomputer time by the NSF Office of Advanced Scientific Computing on the CRAY 2 at the Minnesota Supercomputer Center.

[b] Current address: Institute for Physical Science and Technology and Department of Chemistry and Biochemistry, University of Maryland, College Park, MD 20742.

It is clear that an important aim of our theory of an excess electron in polar solvents is to account for the observed optical absorption spectrum. This involves being able to obtain real time information. Although it has been shown recently that one can in principle simulate electronic absorption spectra using path integral techniques,[13] this has not been applied to complex systems. The situation involving the hydrated electron is even more delicate because of the lack of knowledge of the Hamiltonian describing the excited state. Thus the validity of simulation results can only be inferred by comparing them to the experimentally determined structure of the hydrated electron. Unfortunately, there has been no experiment at room temperature that directly determines the structural properties of the hydrated electron. However, Kevan and co-workers[14–17] have used electron spin resonance (ESR) line shape studies of trapped electrons in γ-irradiated alkaline glass to infer the geometrical structure of the localized electron. The earlier experiments were done in 10 M, ^{17}O enriched alkaline ice glass. By performing a second moment analysis of the ESR line shape and using several approximations these authors inferred the geometry of the trapped electron. According to them, the electron is surrounded by six water molecules arranged with their oxygens and nearest hydrogens forming an octahedron. The nearest hydrogens were determined to be 2.1 Å away from the electron, implying that the next nearest neighbor protons are 3.5 Å away. They also argued that the OH bond of the six water molecules is oriented toward the electron. This was in sharp contrast to all previous models in which it was assumed that in the hydrated electron, the molecular dipole is oriented toward the trapped electron. In order to assess the role of the presence of large amounts of NaOH, Lin and Kevan[17] performed another ESR study of the trapped electron. In this experiment, they co-deposited sodium and water vapor at 77 K. This technique enabled them to keep the concentration of sodium to less than 0.01 M. Although the experimental uncertainty under these conditions was quite a bit larger than in the earlier study they argued that this did not invalidate the earlier picture of the trapped electron. It was also suggested that because the concentration of Na does not seem to affect the geometry of the trapped electron, the inferred geometry could be a realistic representation of an electron solvated in liquid water at room temperature. Given the experimental conditions and the delicate analysis required to infer the geometry of the trapped electron, it is not clear that the structure of the electron localized in alkaline ice glass at 77 K should be the same as that found in liquid water at 298 K. It is for these reasons that the simulations reported in this article and elsewhere[18–20] are important. Our simulations, for the chosen model potential, provide a detailed look at the structure of the hydrated electron and describe in detail the response of the water to the presence of the electron.

On the theoretical side, there have been numerous models that have been proposed to account for the wealth of experimental data.[1–3] However, there have been relatively few which have explicitly taken the molecular structure of the solvent into account. The most notable attempt is due to Newton[21] who used a semicontinuum approach within *ab initio* molecular quantum mechanics to study many facets of electron solvation in polar solvents. In this pioneering work, Newton was able to calculate the equilibrium solvent shell geometry, solvation energy as well as spin densities (which are relevant for ESR experiments) for an excess electron in both water and ammonia. In essence, Newton performed a self-consistent field calculation using the unrestricted Hartree–Fock formalism (UHF) for a discrete cluster of four water molecules containing the excess electron all embedded in a dielectric continuum. Such an approach becomes more accurate as the number of molecules in the cluster is increased. In his study Newton considered both the dipole oriented as well as OH-bond oriented clusters containing four water molecules. These calculations showed that the dipole oriented tetramer embedded in the continuum is more stable by 0.27 eV compared to the corresponding bond oriented tetramer. The cavity radius was calculated to be about 2.6 Å. Newton's calculations are not definitive because the number of water molecules was taken to be four. In addition it is not clear whether the treatment of the many electron problems at the UHF level is adequate to answer some of the subtle questions pertaining to the hydrated electron. It would be interesting to carry out these calculations for larger clusters buried in the continuum using Newton's methods.

This paper is organized as follows. In Sec. II the theory underlying the simulations is presented, an electron–water pseudopotential is described, and a scheme is described in detail to treat the long range polarization contribution of the medium self-consistently. The simulation details are presented in Sec. III. The results are presented in Sec. IV. Our results are then compared with the results of other path integral simulations of similar systems.[18–20] The paper concludes in Sec. V with a discussion of remaining problems.

II. THEORY

A. Path integral Monte Carlo

Consider an excess electron interacting with N water molecules. Assuming that all the particles interact via pairwise potentials the Hamiltonian for such a system can be written as

$$H=\frac{\mathbf{p}^2}{2m}+\sum_{i=1}^{N}\sum_{\alpha=1}^{3}\frac{\mathbf{P}_{i(\alpha)}^2}{2M_\alpha}+\sum_{i<j}V(\mathbf{R}_i,\mathbf{R}_j)+\sum_{i=1}^{N}U(\mathbf{r},\mathbf{R}_i), \tag{1}$$

where $\mathbf{R}_i$ denotes the collection of the coordinates of the ith water molecule, $\mathbf{r}$ is the position of the excess electron, $\mathbf{p}$ is the momentum conjugate to $\mathbf{r}$, m is the electron mass, $\mathbf{P}_{i(\alpha)}$ is the momentum of the αth species of the ith water molecule, and M_α is the corresponding mass where $M_1=M_{\text{oxygen}}$ and $M_{2,3}=M_{\text{hydrogen}}$. The potential of interaction, $V(\mathbf{R}_i,\mathbf{R}_j)$, between two water molecules with coordinates $\mathbf{R}_i$ and $\mathbf{R}_j$ is taken to be a central force potential, i.e., it is taken to be the sum of the potentials between oxygen and hydrogen atoms.[22] The internal vibrations of the water molecule are modeled by a set of appropriate Morse potentials.[23] The pseudopotential, $U(\mathbf{r},\mathbf{R}_i)$, describing the interaction between the electron and the water molecule is described in detail in the next subsection. In the simulations the translational motion of the water molecules is treated classically. This is justified because the thermal de Broglie wavelength of even the proton at the temperature of interest here, namely $T=298$ K, is much smaller than that of the electron. The internal vibrations of the water molecule have to be treated quantum mechanically. However, it is expected that the precise treatment of these quantum mechanical degrees of freedom will have negligible effect on the structural properties of the hydrated electron. The quantity of interest is the canonical partition function for the mixed quantum–classical system which may be written as

$$Q=\mathrm{Tr}(e^{-\beta H/P})^P. \tag{2}$$

If P is very large Q can be approximated by $Q \sim Q_P$, where

$$Q_P=\left(\frac{mP}{2\pi\hbar^2\beta}\right)^{3P/2}\left(\frac{M_{\text{oxygen}}P}{2\pi\hbar^2\beta}\right)^{3N/2} \times\left(\frac{M_{\text{hydrogen}}P}{2\pi\hbar^2\beta}\right)^{3N}\int e^{-\beta S_{\text{eff}}}\prod_{i=1}^{N}\prod_{j=1}^{P} d\mathbf{R}_i\, d\mathbf{r}^{(j)}, \tag{3}$$

where the Euclidian action is

$$S_{\text{eff}}=V_{e^- - \mathrm{W}}+V_{\mathrm{W}-\mathrm{W}} \tag{4a}$$

and

$$V_{e^- - \mathrm{W}}=\sum_{j=1}^{P}\left[\frac{mP}{2\hbar^2\beta^2}(\mathbf{r}^{(j)}-\mathbf{r}^{(j+1)})^2 +\frac{1}{P}\sum_{i=1}^{N}U(\mathbf{r}^{(j)},\mathbf{R}_i)\right] \tag{4b}$$

and

$$V_{\mathrm{W}-\mathrm{W}}=\sum_{i<j}V(\mathbf{R}_i,\mathbf{R}_j). \tag{4c}$$

The set $\{\mathbf{r}^{(t)}\}$ denotes the electron coordinates for different Euclidian timepoints. The explicit derivation of the action for the problem is presented in detail elsewhere.[24] Thus in the discretized path integral formulation the system consisting of an electron interacting with N classical water molecules is isomorphic to $N+P$ classical particles moving in an effective potential field given by Eq. (4). This formulation becomes exact only in the limit of P becoming infinite. In practice a sufficiently large value of P is chosen such that the partition function (and other properties) change negligibly on a further increase of P.

B. Electron–water pseudopotential

To proceed, the explicit form of the potential of interaction between the electron and the water molecule is required. Unfortunately there has been no complete calculation of the potential energy surface, $U(\mathbf{r}, \mathbf{R}_i)$, even at the Hartree–Fock level.[25] In view of this difficulty, and because the nature of localization of the excess electron depends critically on its interaction with the solvent, a fairly reliable pseudopotential is required. Jonah *et al.*[19] have used a potential based on a point charge model. Such an approach is certainly reasonable and indeed sheds light on the need (or lack of it) of a more sophisticated pseudopotential. However, this model is overly simple. It leaves out the long range polarization potential which may well be important in polarizable solvents. Jonah *et al.* have used path integral molecular dynamics in their work. The e^-–water potential, modeled as a point charge–interaction with suitable cutoff to eliminate the Coulomb catastrophe, has also been used by Sprik *et al.*[18] In constructing the potential $U(\mathbf{r}, \mathbf{R}_i)$ we have used an effective potential approach which has enjoyed considerable success in predicting electron–atom as well as electron–molecule scattering over a wide range of impact energies.[26,27] A closely related approach has been employed by Schnitker and Rossky.[20] Although similar, the details of the potential models do differ. In addition we treat many body polarization interactions which are ignored in all other studies.

It is worth remembering that the interaction of the electron with the water molecule is complex and is in general solvable only with many-body *ab initio* techniques. Furthermore, the potential energy surface is nonlocal in space and is also in general dynamic (energy dependent). For the purpose of path integral Monte Carlo simulations it is most convenient to adopt a pseudopotential that is not only local in the coordinate representation but is also independent of energy. In the spirit of the effective potential approach[26,27] it is convenient as well as accurate to represent the many-body interaction of the electron with the target by an equivalent one-body interaction for a fixed value of $\mathbf{R}_i$. This involves an explicit integration over the coordinates of the target electron coordinates for a fixed value of the nuclear coordinates of the target. The effective potential, often referred to as the optical potential,[27] can be written as the sum of four parts. The static potential V^S represents the electrostatic interaction between the incident electron and the unperturbed ground electronic state of molecule charge distribution. The exchange potential V^E takes into account the indistinguishability of the excess electron and the bound electrons of the target. The effect of the charge polarization of the water molecule is represented by the polarization of the target, V^P. The final term is a repulsive term V^R which takes into account the constraint that the one-electron wave function of the excess electron be orthogonal to the target wave function. It is clear that the potential is energy dependent but is usually evaluated in the limit of zero energy, and can be expressed as

$$U(\mathbf{r},\mathbf{R}_i)=V^S+V^E+V^P+V^R. \tag{5}$$

The electrostatic potential V^S is,

$$V^S=e^2\int d\{\mathbf{r}_i\}\frac{\rho(\{\mathbf{r}_i\})}{|\mathbf{r}-\mathbf{r}_i|},$$

where $e\rho(\{\mathbf{r}_i\})$ is the charge distribution given by the square of the molecular wave function of the target, and $\{\mathbf{r}_i\}$ denotes the coordinates of the bound electrons of the target. However, as shown by *ab initio* quantum mechanic calculations, the charge density is concentrated close to the nuclei and thus we approximate V_s by

$$V^S(\mathbf{r}, \mathbf{R}_i) = \frac{2Z_e e}{|\mathbf{r} - \mathbf{R}_\mathrm{O}^i|} - \frac{Z_e e}{|\mathbf{r} - \mathbf{R}_{\mathrm{H}_1}^i|} - \frac{Z_e e}{|\mathbf{r} - \mathbf{R}_{\mathrm{H}_2}^i|}, \tag{6}$$

where $\mathbf{R}_\mathrm{O}^i$, $\mathbf{R}_{\mathrm{H}_1}^i$, and $\mathbf{R}_{\mathrm{H}_2}^i$ are the location of the oxygen atom and the two hydrogen atoms of the ith water molecule. The excess charge Z_e in the central force model is 0.329 83e.

The exchange term, which is a nonlocal term, is usually approximated by a suitable local potential. Various approximations, most of which originated from Slater's free electron gas theory,[28] have been used in electron scattering theory.[29] This term is important when the electron is close to the water molecule. However, in this region the static potential dominates and it is found that the exchange term, given by the Slater theory gives a negligible contribution, can thus be ignored in Eq. (5).

The third term V^P is the polarization potential which becomes important when the electron is sufficiently far away from the water molecule. We only keep the electron-induced dipole interaction which contributes most significantly to the polarization potential. The charge polarization term is also energy dependent. But because of the very low energies (typically thermal energies) encountered here it is appropriate to use the adiabatic approximation in evaluating the polarization potential. The potential V^P is smoothly cut off at small electron–molecule separations to avoid divergences by using a switching function. This is not likely to affect the potential energy surface because at these distances other terms, namely V^S and V^R, dominate over V^P. Thus the form of the polarization potential used in our model is

$$V^P(\mathbf{r}, \mathbf{R}_i) = -\frac{\alpha_0 S(|\mathbf{r} - \mathbf{R}_\mathrm{O}^i|)}{2|\mathbf{r} - \mathbf{R}_\mathrm{O}^i|^4}, \tag{7a}$$

where $S(r)$ is taken to be

$$S(r) = (1 - e^{-r/r_c})^6. \tag{7b}$$

In Eq. (7a) α_O is the spherical dipole polarizability of the water molecule taken to be 1.444 Å^{3}and $S(r)$ is a switching function which smoothly cuts off the polarization potential at small distances. The switching function in Eq. (7) has often been used in low energy electron atom and electron molecule scattering with moderate success.[30] It is customary to choose the range of the switching function r_c by appealing to some prominent feature in the energy dependence of the cross section.[26] Alternatively, Burke and Chandra[31] and Truhlar *et al.*[32] have suggested that r_c be taken as the bond length or the size of the molecule. Accordingly we have taken $r_c = r_\mathrm{OH}^\mathrm{eq}$, where $r_\mathrm{OH}^\mathrm{eq}$ is the equilibrium oxygen–hydrogen bond length of the water molecule.

The last term in our pseudopotential V^R accounts for the orthogonality of the wave function of the excess electron (represented as a plane wave) to the wave function of the water molecule in the ground electron state. The ground state of the water molecule is represented by a multicenter wave function, making the evaluation of an analytical tractable expression quite difficult. In order to simplify this problem, we assume that the multicenter wave function can be expressed as a sum of terms each centered around the three nuclei. This is similar to the one-center expression which has been used to calculate static potentials for AH_n molecules.[33,34] The static potentials thus calculated have been shown to be accurate except close to the nuclei. In this approximation the repulsive term V^R becomes

$$V^R(\mathbf{r}, \mathbf{R}_i) = V_R^\mathrm{O}(\mathbf{r}, \mathbf{R}_\mathrm{O}^i) + V_R^\mathrm{H}(\mathbf{r}, \mathbf{R}_{\mathrm{H}_1}^i) + V_R^\mathrm{H}(\mathbf{r}, \mathbf{R}_{\mathrm{H}_2}^i), \tag{8}$$

where $\mathbf{R}_\mathrm{O}^i$, $\mathbf{R}_{\mathrm{H}_1}^i$, and $\mathbf{R}_{\mathrm{H}_2}^i$ are the coordinates of the oxygen and the hydrogen atoms of the ith water molecule. For $V_R^\mathrm{H}(\mathbf{r}, \mathbf{R}_{\mathrm{H}_1}^i)$ we use the following expression (in atomic units):

$$V_R^\mathrm{H}(\mathbf{r}, \mathbf{R}_{\mathrm{H}_1}^i) = 0.185 e^{-|\mathbf{r} - \mathbf{R}_{\mathrm{H}_1}^i|/a_0} + Z_e e \frac{e^{-|\mathbf{r} - \mathbf{R}_{\mathrm{H}_1}^i|/a_0}}{|\mathbf{r} - \mathbf{R}_{\mathrm{H}_1}^i|}, \tag{9}$$

where a_0 is the Bohr radius. A similar expression holds for $V_\mathrm{R}^H(\mathbf{r}, \mathbf{R}_{\mathrm{H}_2}^i)$. For the core repulsion centered on the oxygen atoms we adopt a simple exponential for

$$V_R^\mathrm{O}(\mathbf{r}, \mathbf{R}_\mathrm{O}^i) = V_0 e^{-|\mathbf{r} - \mathbf{R}_\mathrm{O}^i|/r_\mathrm{OH}^\mathrm{eq}}, \tag{10}$$

where $V_0 = 0.046\,793\,E_\mathrm{H}$. We have calculated V_R^O using the double zeta (minimal basis set) of Clementi and have found that there is no significant change in the resulting electron–water potential energy surface.[35]

The total potential energy surface, which we will refer to as model potential I, is given by the sum of terms given in Eqs. (5)–(10). In Fig. 1, we plot the potential energy contour for the fixed equilibrium geometry of the water molecule. The pseudopotential thus obtained is not expected to

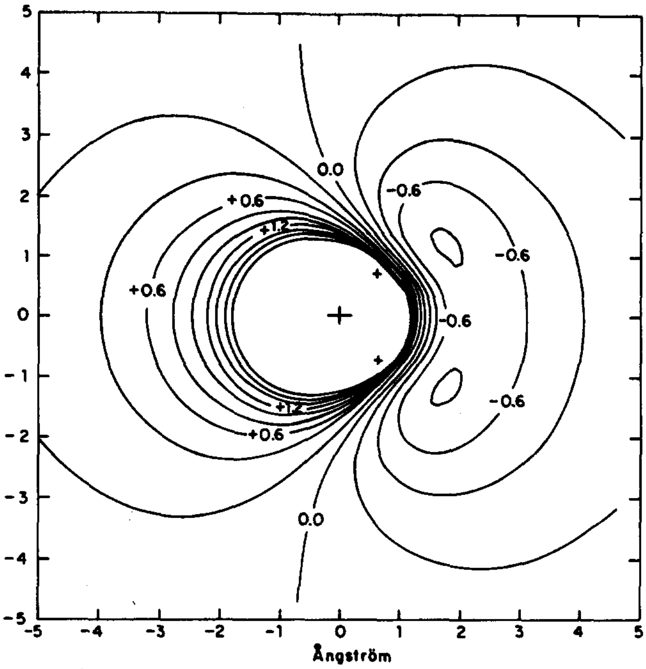

FIG. 1. Potential energy contours of the electron water potential for model potential I. This figure shows the electron water energy in the bisector plane of the water molecule in its equilibrium geometry. The well depth at the hydrogen atoms are approximately 0.8 eV. The contour increment indicates a change of 0.2 eV.

properly reproduce the cusps near the nuclei. This is probably not important for our simulations because we are dealing with very low energy electrons. The figure shows that the potential has a minima at the bond oriented geometry, i.e., as the electron approaches along the oxygen–hydrogen bond axis. The value of the minimum in the potential is about -0.8 eV.

The qualitative features of this potential energy surface seem similar to that found by Schnitker and Rossky.[20] However, the well depth of their potential energy surface is about twice our value. This larger well depth is due to the difference in the models for water used by these authors and the one used here. Schnitker and Rossky used the SPC model for water in which charges on the oxygen (and thus the hydrogens) are adjusted so that the effective dipole moment of a water molecule in liquid water is correctly obtained. This value is larger than the value appropriate for an isolated water molecule used here. The charge assignment in the central force model of water is consistent with the dipole moment of a monomer. Our approach has been to obtain an electron–water pseudopotential using the well-known ground-state quantum mechanical properties of an isolated water molecule and to use such a potential for an electron in liquid water. Thus all the parameters characterizing our model potential are consistent with the properties of the isolated water molecule.

Although it is true that in bulk water the ionicity of the O–H bond is increased over the gas phase, the waters surrounding the electron cavity do not feel the full dielectric response found in bulk water. These water molecules may then not have the same charges as in bulk water. Thus we expect that the true pseudopotential for an electron in water will lie somewhere between ours and Schnitker and Rossky's potential.

C. Self-consistent treatment of polarization effects

The long range polarization effect given by the approximate adiabatic polarization potential [cf. Eq. (7)], is only valid when the electron interacts with an isolated water molecule. When the excess electron is in liquid water, many-body polarization effects can become important and their inclusion will modify the effective action used in the path integral Monte Carlo simulations. This subsection describes the quantum mechanical treatment of many body polarization. Stillinger and David[36] introduced a class of polarization models to describe classical ion solvation in small clusters of water. Our quantum treatment of the many body polarization effect makes use of a similar approach.

The excess electron induces a dipole moment on each water molecule. In our model, a dipole polarizability is associated with each oxygen atom. Assuming, for the moment, that the excess electron is a classical particle, the additional dipole moment induced on the oxygen atom of the ith water molecule is given by classical electrostatics as

$$\mu_{iO} = \alpha_O \mathbf{G}_i, \tag{11}$$

where $\mathbf{G}_i$ is the external electric field due to the excess electron and all other induced dipole moments. The vector field $\mathbf{G}_i$ is explicitly given by

$$\mathbf{G}_i = \frac{e\mathbf{r}_{iO} S_1(|\mathbf{r}_{iO}|)}{|\mathbf{r}_{iO}|^3} - \sum_{\substack{k=1\\k\neq i}}^{N} \frac{\overleftrightarrow{\mathbf{T}}_{ik}\cdot\mu_{kO} S_1(|\mathbf{r}_{ik}|)}{|\mathbf{r}_{ik}|^3}, \tag{12}$$

where the second term in the above equation is the induced dipole–induced dipole interaction between the ith and kth water molecule and $\overleftrightarrow{\mathbf{T}}_{ik}$ is given by

$$\overleftrightarrow{\mathbf{T}}_{ik} = 1 - \frac{3\mathbf{r}_{ik}\mathbf{r}_{ik}}{|\mathbf{r}_{ik}|^2}, \tag{13}$$

where $|\mathbf{r}_{ik}|$ is the distance between the oxygen atoms of the ith and kth water molecule and $\mathbf{r}_{iO} \equiv \mathbf{r} - \mathbf{R}^i_O$. The function $S_1(r)$ in Eq. (12) is an appropriate switching function which partially accounts for the diffuse nature of the charge distribution around the oxygen atom, thereby giving rise to a dipole polarizability that depends on r. For a purely classical particle this function would be unity. With a switching function that rapidly changes over the size of the water molecule, the many body polarization potential can be determined. For a given value of $\mathbf{r}$ and the coordinates of all the water molecules $\{\mathbf{R}\}$ the set of linear equations (11) and (12) can be solved for μ_{iO} ($i = 1,2,\ldots,N$). Having obtained μ_{iO} the polarization potential is given by

$$\Phi_{\text{pol}}(\mathbf{r}, \{\mathbf{R}\}) = -\frac{e}{2}\sum_{i=1}^{N} \frac{\mu_{iO}\cdot\mathbf{r}_{iO} S(|\mathbf{r}_{iO}|)}{|\mathbf{r}_{iO}|^3}. \tag{14}$$

In our simulation we choose $S_1(r)$ to be the switching function $1 - K(r)$ as defined in the work of Stillinger and David. The $\Phi_{\text{pol}}(\mathbf{r}, \{\mathbf{R}\})$ is turned off at close distances by $S(r)$, Eq. 7(b), so as to ensure that the expressions (14) and (7a) reduce to each other for the isolated water molecule interacting with an electron. The effect of $S_1(r)$ was found to be negligible.

The quantum generalization of the above classical self-consistent treatment of charge polarization effects, with the water molecules treated classically, is simple. According to the isomorphic picture[37] the quantum system is equivalent to a classical ring polymer consisting of P electron beads interacting with N water molecules. The tth electron bead and all the induced dipoles on the other water molecules (except the ith water molecule) induce a dipole moment on the ith water molecule, given by

$$\mu_{iO}^{(t)} = \alpha_O \mathbf{G}_i^{(t)}. \tag{15}$$

The vector field $\mathbf{G}_i^{(t)}$ becomes

$$\mathbf{G}_i^{(t)} = \frac{e\mathbf{r}_{iO}^{(t)} S_1(|\mathbf{r}^t_{iO}|)}{|\mathbf{r}^t_{iO}|^3} - \sum_{\substack{k=1\\k\neq i}}^{N} \frac{\overleftrightarrow{\mathbf{T}}_{ik}^{(t)}\cdot\mu_{kO}^{(t)} S_1(|\mathbf{r}_{ik}^{(t)}|)}{|\mathbf{r}_{ik}^{(t)}|^3}, \tag{16}$$

where $\overleftrightarrow{\mathbf{T}}_{ik}^{(t)}$ is given by Eq. (13). Once again Eqs. (15) and (16) are solved for $\mu_{iO}^{(t)}$ $t = 1,2,\ldots,P$ and for $i = 1,2,\ldots,N$. The contribution of the many-body polarization energy to the effective action S_{eff} is then given by

$$\Phi_{\text{pol}}^{(q)}(\{\mathbf{r}^{(t)}\},\{\mathbf{R}\}) = -\frac{e}{2P}\sum_{t=1}^{P}\sum_{i=1}^{N} \frac{\mu_{iO}^{(t)}\cdot\mathbf{r}_{iO}^{(t)} S(|\mathbf{r}_{iO}^{(t)}|)}{|\mathbf{r}_{iO}^{(t)}|^3}. \tag{17}$$

The pseudopotential obtained by using Eq. (17) instead of Eq. (7) for the polarization is the second (II) model potential. In the Monte Carlo simulation one has to calculate $\Phi_{\rm pol}^{q}(\{\mathbf{r}^{(t)}\},\{\mathbf{R}\})$ by solving Eqs. (15) and (16) at each iteration. In an actual simulation it is appropriate to count only those water molecules which are within a cutoff distance of the t th electron bead. We choose this cutoff distance R_c to be about 5.5 Å and at each step about a third of the water molecules were included in calculating $\Phi_{\rm pol}^{(q)}(\{\mathbf{r}^{(t)}\},\{\mathbf{R}\})$. The matrix equation, for the induced dipole moments, was solved by using an iterative scheme. This is faster than inverting the entire matrix at each step of the simulation.

III. SIMULATION DETAILS

Within the path integral formulation, outlined in Sec. II A, the calculation of the partition function is reduced to the evaluation of a multidimensional integral, Eq. (3). The structure of this integral quickly reveals certain problems which arise as the number of beads P on the electron polymer chain increases. If one were to make single particle moves (as is normally done in the primitive algorithm) using the Metropolis Monte Carlo technique, it is clear that the stiffness of the polymer will allow only very small moves.[38] Thus configuration space will be covered very slowly. This problem will become particularly severe as P increases because it is known from simulations of polymers that the Rouse relaxation time[39] is approximately proportional to P^2. To some extent this problem has been overcome within the primitive algorithm by resolving the chain modes into normal modes and by moving each mode according to the appropriate force constant.[40] In addition, the movement of the center of mass of the ring polymer (corresponding to the zero frequency normal mode), seems to enhance the acceptance probability. However, it does appear that when P exceeds several hundreds (typically 400 or so) these modifications of the primitive algorithm are not sufficient to overcome the inefficiencies in the sampling scheme. A similar argument can be made about molecular dynamics path integral simulations based on the primitive algorithm. In the work reported here we have adopted a scheme for generating *a priori* transition probabilities suggested by several workers.[41,42] The basic idea behind the algorithm is simple: the density matrix between the two end points is written as a product of normalized conditional probabilities. These transition probabilities provide criteria for picking the next state point (configuration) given the present state point and the end point. A useful approximation for these conditional probabilities, which is valid if $\epsilon = \beta/P$ is sufficiently small, can be found by expanding about the present configuration. The *a priori* transition probability is a Gaussian with the exponent in the Gaussian depending on a drift term. The drift term contains the interaction of the particle with the environment. For details of this algorithm with application to low temperature liquid ^{4}He (without exchange effects) the reader is referred to the original article.[41] To further enhance the sampling efficiency we have neglected the drift term. When dealing with electron solvation, this seems to be more efficient and the empirical justification for this comes from a detailed study of an excess electron in a He cavity at several densities.[43]

In our simulations, there are 216 classical water molecules at a density of $\rho = 1.0$ g/cc, and at temperature $T = 298$ K. The water molecules and the excess electron were enclosed in a cubic box of length 18.6 Å. As usual, periodic boundary conditions were employed to eliminate surface effects. The number of beads on the electron ring polymer was varied from $P = 90$ to $P = 900$. The convergence of the results with increasing P is discussed in detail in the Appendix. In the staging algorithm used here a segment of the chain is snipped and moved to a new position by sampling according to the Gaussian transition probability.[43] The length of the chain segment was taken to be 5 for $P = 90$, 20 for $P = 450$, and 40 for $P = 900$. This choice of chain segment length was made to optimize the transition probabilities. Each move of the water molecule involved the displacement of the center-of-mass of the molecules, vibration of the atoms, etc. The step sizes were adjusted to yield an acceptance probability of about 30% for both the solvent molecules and the electron ring polymer. For the $P = 900$ case an equivalent of about 48 000 passes was used. These long runs were necessary to insure convergence of the results.

The size of the cubic box in our simulations is 18.6 Å and this is not much larger than the thermal de Broglie wavelength of the electron at room temperature which is 17.1 Å. The size of the electron and the long range of the electron–water interaction (see the static potential V^S) implies that one probably has to use Ewald summation. However, because the electron seems to localize rapidly to a small region of about 8 Å^3 in volume these long range effects are expected to be screened efficiently. In systems where the states of the electron are more delocalized, finite size effects may become important.

The algorithm was coded and developed for optimal performance on a single processor vector machine. The code is described elsewhere[44] and its performance evaluated for a number of computers. The runs described here were performed on a CRAY 2 supercomputer.

IV. RESULTS

The presentation of the results is organized into two subsections. In Sec. IV A, the structural aspects of the solvated electron are analyzed and in Sec. IV B we discuss the energetics of the problem. The results are presented for both of the model potentials: the first model (I) is based on the potential energy surface given by Eqs. (5)–(10) whereas the second model (II) is based on the self-consistent treatment of the polarization potential [cf. Eqs. (15)–(17)]. These results are all based on simulations with $P = 900$. Convergence is discussed in the Appendix.

A. Structural aspects

In order to elucidate the structure of the solvated electron, various correlation functions have been calculated. By studying the behavior of these correlation functions a coherent picture of the hydrated electron emerges. It is of importance to remember that potential model I corresponds to pairwise additivity of the polarization potential whereas model II corresponds to a self-consistent treatment of the many-body polarization forces.

What is the structure of the water molecules around the electron? This is most easily answered by calculating the radial distribution functions of the hydrogen and the oxygen atoms measured with respect to the barycenter of isomorphic electron polymer, i.e.,

$$g_{e^-_{\rm com}\text{-H}}(r) = \left\langle \delta\left(r - R_{\rm H} + \frac{1}{P}\sum_{t=1}^{P} r^{(t)}\right)\right\rangle. \qquad (18)$$

A similar expression holds for the corresponding electron center-of-mass oxygen radial distribution function, $g_{e^-_{\rm com}\text{-O}}(r)$. The averages involving the electron center-of-mass quantity are expected to be less accurate due to the limited amount of sampling possible with only one barycenter. In addition we have also calculated the true electron–hydrogen radial distribution function which is given by

$$g_{e^-\text{-H}}(r) = \frac{1}{P}\left\langle \sum_{t=1}^{P} \delta(r - R_{\rm H} + r^{(t)})\right\rangle. \qquad (19)$$

The true electron–oxygen radial distribution function, $g_{e^-\text{-O}}(r)$, is given by a similar expression. In Fig. 2(a) a plot of the $g_{e^-_{\rm com}\text{-O}}(r)$ for the two-model potentials as a function of r is shown. There are several features that are worth noting. The peak heights of both the curves are much smaller than would be expected for the well-defined structure often seen in classical ion solvation.[45,46] The height of the first peak in the solvated electron [see Fig. 2(a)] is 1.3 whereas in the case of small ion solvation the height is near 3.0. It is apparent that there is no perceptible structure seen in the second solvation shell. There are two significant differences between $g^{\rm I}_{e^-_{\rm com}\text{-O}}(r)$ corresponding to potential I and $g^{\rm II}_{e^-_{\rm com}\text{-O}}(r)$ corresponding to potential II. The striking feature in Fig. 2(a) is that in the region around 2.0 Å, $g^{\rm II}_{e^-_{\rm com}\text{-O}}(r)$ is pushed outward by about 0.5 Å as compared to $g^{\rm I}_{e^-_{\rm com}\text{-O}}(r)$. This implies that the electron excludes a larger region when the effect of the polarization is treated self-consistently and consequently there is a clear increase in the effective hard-core diameter of the electron. Secondly, although both curves do not show appreciable structure it is apparent that the first peak of $g^{\rm II}_{e^-_{\rm com}\text{-O}}(r)$ is higher and narrower than that seen in $g^{\rm I}_{e^-_{\rm com}\text{-O}}(r)$. Furthermore, the location of the *peak height* in $g^{\rm II}_{e^-_{\rm com}\text{-O}}(r)$ is shifted inward by about 0.3–0.4 Å as compared to the corresponding distance in $g^{\rm I}_{e^-_{\rm com}\text{-O}}(r)$. The distribution function obtained using model potential I is much broader suggesting that the many body effects in potential II makes the electron behave more like a classical ion.

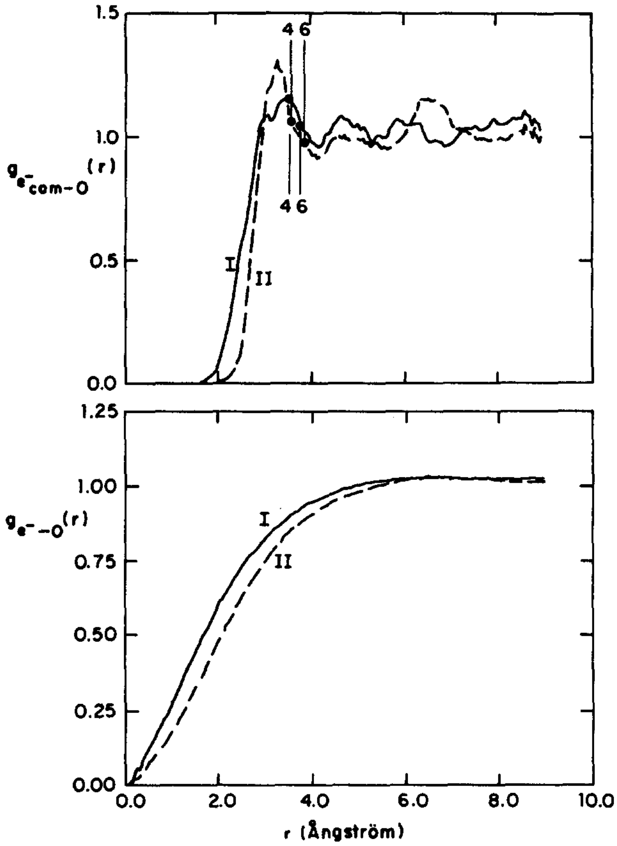

FIG. 2. (a) Top: The pair correlation function $g_{e^-_{\rm com}\text{-O}}(r)$ as a function of r is shown for the two model potentials for $P = 900$. The solid line, corresponding to model potential I extends further in towards the electron center of mass than for model potential II, which is shown in the broken line. The region beyond 4 Å does not show any structure above the noise level. Also indicated is the running coordination number of four and six for both potentials, bottom row gives the values for potential I and the top row for potential II. (b) Bottom: The true electronic pair correlation function $g_{e^-\text{-O}}(r)$ for the two model potentials. Model potential I extends further in towards the oxygen atom on the water molecule than for model potential II. Both correlation functions rise smoothly to 1 at about 4 Å with no evidence for structuring of water molecules around single electron pseudoparticles.

As a comparison to the earlier work on the solvated electron[2,3] it is of interest to obtain an effective one-body potential that the electron experiences in the polar solvent. One can estimate this by inverting the radial distribution function, i.e.,

$$V_{\rm eff} \sim -\frac{1}{\beta}\ln g_{e^-_{\rm com}\text{-O}}(r)$$

and this yields a well depth of about $-0.26\,kT$ ($\sigma = 3.0$ Å) for potential II. The corresponding value for potential I is $-0.15\,kT$ ($\sigma = 2.9$ Å).

The rather clear increase in the effective hard core observed in $g^{\rm II}_{e^-_{\rm com}\text{-O}}(r)$ as compared to $g^{\rm I}_{e^-\text{-O}}(r)$ can be rationalized by estimating the contribution of the repulsive part of the self-consistent polarization given by Eq. (17). We assume that the charge is located essentially at the center of the electron ring polymer. Furthermore assuming that (i) the induced dipole moments on all the water molecules are identical (a mean-field approximation), (ii) the average effective distance of the oxygen atoms from the electron barycenter is 3 Å, and (iii) on the average all the induced dipoles are pointing in the same direction, the repulsive contribution can be shown to be equal to

$$U_R \sim \frac{\mu^2 N_{\rm eff}(N_{\rm eff}-1)\cos^2(\theta)}{16\langle r_{e^-_{\rm com}\text{-O}}\rangle^3}.$$

For $N_{\rm eff} = 6$, $\cos(\theta) \sim \frac{1}{2}$ [which seems reasonable and is suggested by $P_D(\theta)$, shown below], and $\langle r_{e^-_{\rm com}\text{-O}}\rangle = 3$ Å it turns out that $\mu \sim 0.383$ D and the above equation yields $U_R \sim 0.1\,kT$. This increased repulsion arises from the following: The electron induces a dipole in a water molecule which in turn induces an antiparallel dipole in a nearest neighbor shell water molecule. The latter dipole points away

TABLE I. Energy terms for various quantities of the electron water system. E_{H_2O} denotes the potential energy due to the internal distortions of a single water molecule. Water energies given in kcal/mol *water* and electron energies in kcal/mol *electron*. The variance is given in parentheses. The kinetic energy was calculated using the virial estimator (Ref. 40).

	Potential I	Potential II
$E_{H_2O\text{-}H_2O}$	-10.15 (0.22)	-10.05 (0.23)
E_{H_2O}	$+1.27$ (0.07)	$+1.28$ (0.07)
$E_{e^-\text{-}H_2O}$	-65 (18)	-63 (18)
Kinetic E	$+23$ (8)	$+20$ (8)

from the electron and thus gives rise to a repulsion. Considering that the effective well depth is about $-0.26\ kT$ and noting that the effective repulsion is about 20% of the absolute value of the electron–water interaction (see Table I) it seems plausible that the effective hard-sphere diameter can increase by about 0.5 Å when the many-body polarization potential is treated self-consistently. This does not imply that the net electron–water interaction for potential II is larger (more repulsive) than for potential I. In order to give a more accurate assessment of the effect of the self-consistent treatment of the many body polarization potential one should solve an approximate integral equation within the quantum mean-field approximation.

The lower panel, Fig. 2(b), shows the true electronic distribution, $g_{e^-\text{-O}}(r)$. This shows that there is a definite exclusion region with the size of the region being bigger in $g^{\mathrm{II}}_{e^-\text{-O}}(r)$ than in $g^{\mathrm{I}}_{e^-\text{-O}}(r)$. These curves will be structureless even if there is a well-defined cavity with strong correlations because one is averaging over all beads. The electron density extends into the neighboring water molecules penetrating to about 0.15 Å from the oxygens. The total contribution to the potential energy from the electrons in the region inside the atomic cores is very small due to the low electron density there. If a more repulsive electron–oxygen potential was used the electron would not get as close to the oxygen atom.

The electron–hydrogen radial distribution functions are shown in Fig. 3. Figure 3(a) shows that the radial distribution functions measured with respect to the center-of-mass of the electron ring polymer, $g^{\mathrm{I}}_{e^-_{\mathrm{com}}\text{-H}}(r)$, penetrates about 0.9 Å further in than $g^{\mathrm{I}}_{e^-_{\mathrm{com}}\text{-O}}(r)$. The hard core of the electron barycenter hydrogen distribution function is smaller than the electron barycenter oxygen distribution by about the equilibrium oxygen–hydrogen bond length. This is an indication that the water molecules are coordinated with the OH bonds pointing towards the electron. Figure 3 shows clearly the difference between $g^{\mathrm{I}}_{e^-_{\mathrm{com}}\text{-H}}(r)$ and $g^{\mathrm{II}}_{e^-_{\mathrm{com}}\text{-H}}(r)$. The radial distribution function $g^{\mathrm{I}}_{e^-_{\mathrm{com}}\text{-H}}(r)$ is quite structureless with hydrogen penetrating closer to the barycenter (by about 0.6 Å) than does $g^{\mathrm{II}}_{e^-_{\mathrm{com}}\text{-H}}(r)$. However, $g^{\mathrm{II}}_{e^-_{\mathrm{com}}\text{-H}}(r)$ shows pronounced structure in the first two peaks centered at 2.5 and 3.5 Å, respectively. The positions of the hydrogen peaks correspond roughly to a structure where one hydrogen of a shell water molecule points towards the electron and the other is hydrogen bonded to a neighboring water molecule. This is shown more clearly below in the discussion of orientational correlation functions. The pronounced structure is consistent with our earlier observation that the model potential II seems to make the electron more like a classical ion. The effective potential felt by the electron is much softer if the many-body polarization potential contributions are ignored. Figure 3(b) shows the true $g^{\mathrm{I}}_{e^-\text{-H}}(r)$ and $g^{\mathrm{II}}_{e^-\text{-H}}(r)$, and reveals that the electron penetrates much closer to the hydrogen in potential I than in potential II. Both potentials allow for the electron to tunnel into the hydrogen atom but again the contribution to the total potential energy is small. A more repulsive electron–hydrogen potential would keep the electrons further away from the hydrogen atom.

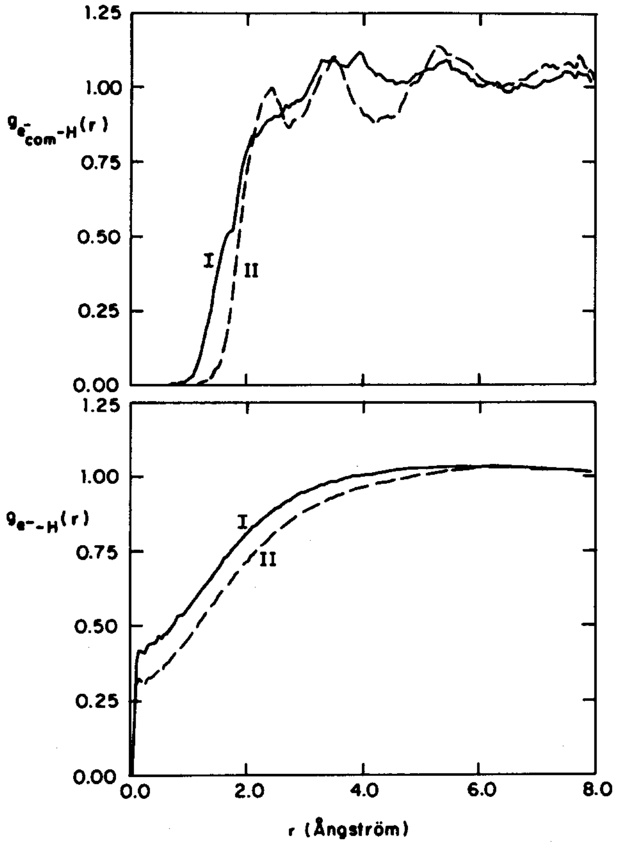

FIG. 3. (a) Top: The pair correlation function $g_{e^-_{\mathrm{com}}\text{-H}}(r)$ is shown for the two model potentials for $P = 900$. The solid line, indicating model potential I, shows appreciable density further in towards the electron center-of-mass than the model potential II, shown in the broken line. Model potential II shows more structure in the shell region, with a well defined first peak at ~ 2 Å, than the corresponding simulation employing model potential I. (b) Bottom: The true electronic pair correlation function $g_{e^-\text{-H}}(r)$ for the two model potentials. Model potential I shows more density close by the hydrogen atoms on the water molecule than for model potential II. Both potentials allow for the electron to penetrate within a few tenths of an angstrom of a hydrogen atom.

In order to understand the local geometry of the water molecules around the electron it is useful to know the coordination number of the water molecules. Accordingly, we calculated the coordination number, $n_{H_2O}(r)$, defined as

$$n_{H_2O}(r) = 4\pi\rho \int_0^r s^2 g_{e^-_{\mathrm{com}}\text{-O}}(s)\,ds \tag{20}$$

and Fig. 4 shows a plot of this quantity as a function of r. Neither $n^{\mathrm{I}}_{H_2O}(r)$ nor $n^{\mathrm{II}}_{H_2O}(r)$ shows evidence for clear structure. A sixfold coordination, necessary for octahedral geometry, is obtained when r is approximately 3.7 Å for both potentials and this is further than the distance of 3.1 Å sug-

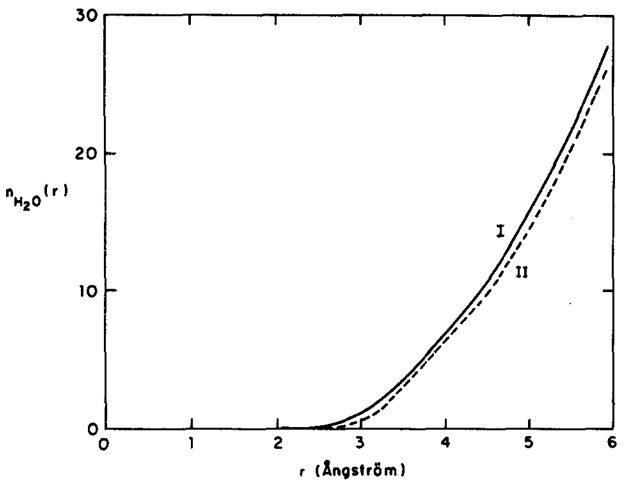

FIG. 4. The running coordination number, $n_{H_2O}(r)$ [defined in Eq. (20)], is shown for the two model potentials. Neither $n^{I}_{H_2O}(r)$ nor $n^{II}_{H_2O}(r)$ shows evidence for a clear water structure around the electron center of mass. A sixfold coordination, necessary for octahedral geometry, is obtained when $r \sim 3.7$ Å for both potentials [see also Fig. 2(a)].

gested by Kevan and co-workers.[16,17]

Further insight into the local geometrical structure of the water molecules may be obtained by calculating two orientational correlation functions. The first one is defined as

$$P_D(\theta) \propto \left\langle \sum_j \delta\left[\hat{R}_{D_j} \cdot \hat{r}_{e^-_{\mathrm{com}\,j}} - \cos(\theta)\right]\right\rangle, \tag{21}$$

where $\hat{R}_{D_j}$ is the unit vector pointing along the dipole of the jth water molecule and $\hat{r}_{e^-_{\mathrm{com}\,j}}$ is the unit vector pointing from the barycenter of the electron polymer to the oxygen atom of the jth water. The second correlation function is defined as

$$P_{\mathrm{OH}}(\theta) \propto \left\langle \sum_j \delta\left[\hat{r}_{\mathrm{OH}_j} \cdot \hat{r}_{e^-_{\mathrm{com}\,j}} - \cos(\theta)\right]\right\rangle, \tag{22}$$

where $\hat{r}_{\mathrm{OH}_j}$ is the unit vector along the oxygen–hydrogen bond *closest* to the electron barycenter of the jth water. From Eqs. (21) and (22) it is clear that the two quantities are dependent on the number of water molecules included in the averaging process and, hence, are dependent on **r**, where **r** is the magnitude of the distance measured with respect to the center-of-mass of the ring polymer. Accordingly we have calculated $P_D(\theta)$ and $P_{\mathrm{OH}}(\theta)$ by including only those water molecules that lie within a shell of 4.5 Å from the electron center-of-mass. In order to examine the influence of the electron in reorienting the solvent molecules in the bulk we have also calculated these orientational correlation functions counting only those solvent molecules in the bulk.

A plot of $P_D(\theta)$ as a function of $\cos(\theta)$ is shown in Fig. 5. Figure 5(a) shows the $P^{I}_D(\theta)$ obtained by considering the water molecules in the shell and bulk, Fig. 5(b) shows $P^{II}_D(\theta)$. The bulk distribution is quite similar for both the model potentials. Both of these distributions are rather broad with $P^{I}_D(\theta)$ showing a maximum at $\theta \sim 75°$ and $P^{II}_D(\theta)$ exhibiting a maximum at $\theta \sim 80°$. When considering the shell region there is a definite structure in $P^{II}_D(\theta)$ and the maximum is shifted to $\theta \sim 53°$ vs the bulk, $\theta \sim 0°$. By comparison the shell and bulk $P^{I}_D(\theta)$ is quite similar. More importantly both $P^{I}_D(\theta)$ and $P^{II}_D(\theta)$ clearly demonstrate that

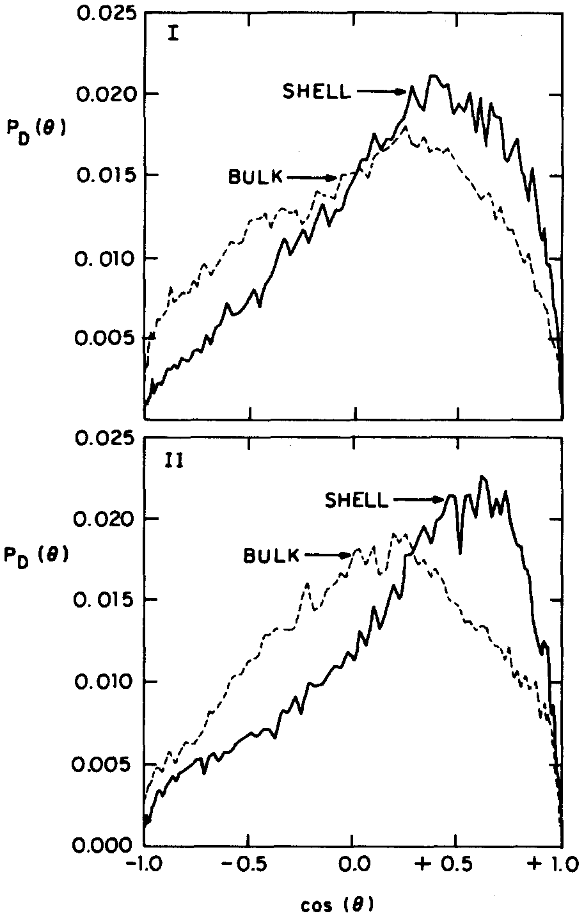

FIG. 5. (a) Top: The orientational correlation function $P_D(\theta)$ as a function of $\cos(\theta)$ for model potential I for shell and bulk regions. If the dipole was pointing towards the electron center-of-mass the distribution would peak at $\cos(\theta) = +1$. The shell region shows a slight tendency to point inwards as compared to the bulk distribution. (b) Bottom: The orientational correlation function $P_D(\theta)$ for model potential II. The shell distribution peaks at an angle closer to perfect dipole alignment than for model potential I.

the solvent molecules around the electron are not strongly dipole oriented, i.e., the water molecules do not have their respective dipole moments pointing towards the electron, with a corresponding peak expected near $\cos(\theta) = 1$. Of course more dipoles point inwards than outwards.

In Fig. 6, we present a plot of $P_{\mathrm{OH}}(\theta)$ as a function of $\cos(\theta)$ for the shell and bulk water molecules. Both $P^{I}_{\mathrm{OH}}(\theta)$ and $P^{II}_{\mathrm{OH}}(\theta)$ clearly show a sharp peak at $\theta \sim 20°$ in the shell. This is clear evidence that the local geometry of water molecules around the electron is more bond oriented than dipole oriented, i.e., the OH bond of the water molecules point inward. This conclusion, although in agreement with the suggestion made by Kevan *et al.*,[16,17] Jonah *et al.*,[19] and Schnitker and Rossky[20] is in contrast to previous theoretical work.[21] It should also be emphasized that $P^{II}_{\mathrm{OH}}(\theta)$ peaks at lower angles than $P^{I}_{\mathrm{OH}}(\theta)$ indicating that the model potential II accentuates the bond oriented geometry.

There is little doubt that the electron forms a cavity in liquid water at room temperatures. The electron ring polymer was started randomly with the beads extending over several water molecules. It was found that such a chain rapidly became quite localized in a region excluding the solvent molecules. Since one sees this cavity formation it is of inter-

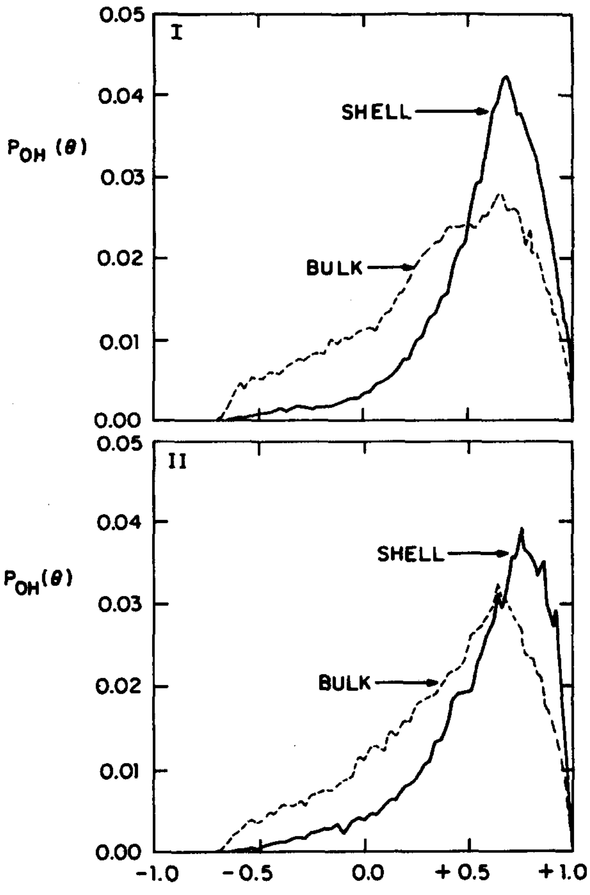

FIG. 6. (a) Top: The orientational correlation function $P_{OH}(\theta)$ as a function of cos(θ) for model potential I for shell and bulk regions. The shell region is clearly peaked at an angle pointing towards the electron center-of-mass. Compared to Fig. 5(a) there is a propensity for the water molecules to orient their OH bonds towards the electron center-of-mass. These distributions are also sharper than the corresponding ones for $P_D(\theta)$ in Fig. 5. (b) Bottom: The orientational correlation function $P_{OH}(\theta)$ for model potential II. The shell distribution of the OH bond vector shows a stronger orientation for the bond to point towards the electron center of mass than model potential I.

est to characterize the geometrical properties of such a cavity. The size of the cavity, which is on the average spherical, can be specified by the electron radius. There are several ways to define the radius and we have adopted the one suggested by Newton,[21] i.e.,

$$\langle R \rangle = \int |r| \rho(r) dr, \qquad (23)$$

where $\rho(r)$ is the electron density, $\rho(r) = \langle \delta(r - r^{(t)} + \frac{1}{P} \Sigma_{t=1}^{P} r^{(t)}) \rangle$. With this definition, it is found that the radius obtained using the model potential I is 2.25 Å while using model II it is 2.11 Å. This indicates that in model I the electron can intrude more into the space between shell water molecules than it can in model II. This is consistent with the stronger effective repulsion in model II. Quite surprisingly these values are in excellent agreement with that found by Jonah *et al.*,[19] who used an entirely different model potential. It should be noted that the earlier studies on the solvated electron also predicted a similar value of the cavity radius.[18,20,47]

Although the electron density distribution appears to be spherical and quite well localized, there are density fluctuations in the solvent that cause fluctuations in the electronic distribution. These fluctuations can therefore distort the spherical shape of the electron ring polymer. In order to assess the deviation from the spherical shape we have computed the average eigenvalues of the electron moment of inertia tensor, measured with respect to the center of mass of the electron ring polymer. The three principle eigenvalues for the model potential I turned out to be 2.10, 1.92, and 2.03 Å whereas the model potential II yields 1.95, 1.80, and 1.89 Å. The radii of gyration of the polymer obtained from these eigenvalues are 2.02 and 1.89 Å for potentials I and II, respectively. Thus the cavity is very close indeed to being spherical in shape and there seems to be negligible deviation from this. In Fig. 7 we show a series of snapshots of the polymer taken at various stages of the simulation. This shows that the electron is localized (recall that the boxlength is 18.6 Å) in a small region of phase space. The shape of the polymer is roughly spherical although there are some deviations from this shape. In order to characterize the fluctuations, which prove to be Gaussian, the variance in the cavity radius was calculated. For both the model potentials, the variance divided by the square radius, i.e., $(\langle R^2 \rangle - \langle R \rangle^2)/$

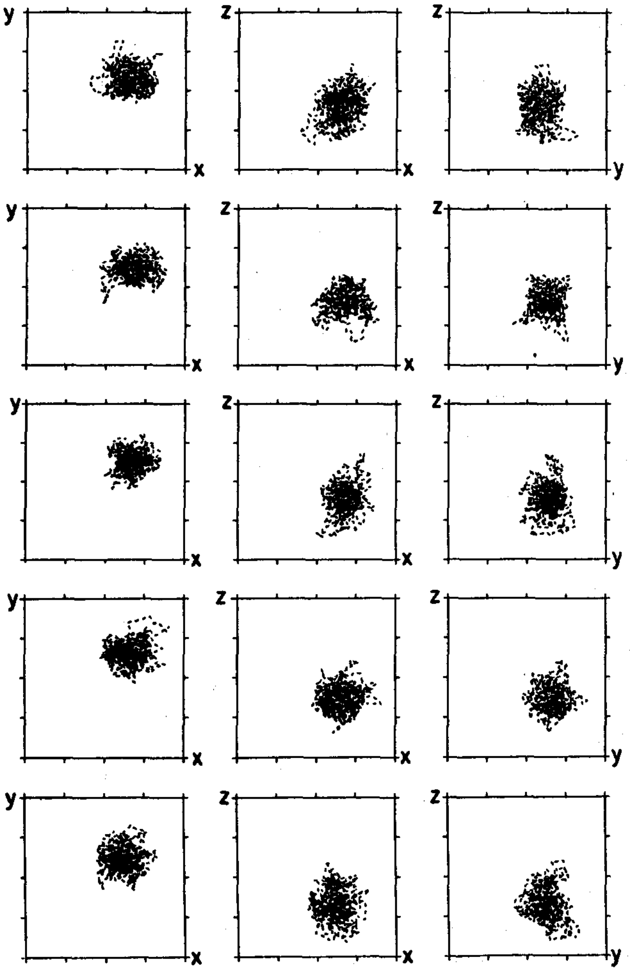

FIG. 7. Snapshots of the electron configurations projected along the *xy*, *xz*, and *yz* axis, the water molecules are not drawn for clarity. Each snapshot is taken at an interval of 8000 passes of the simulations with model potential I. The electron is roughly spherical in shape. There are "fingers" of electron densities extending beyond the immediate water molecules in the shell around the electron cloud.

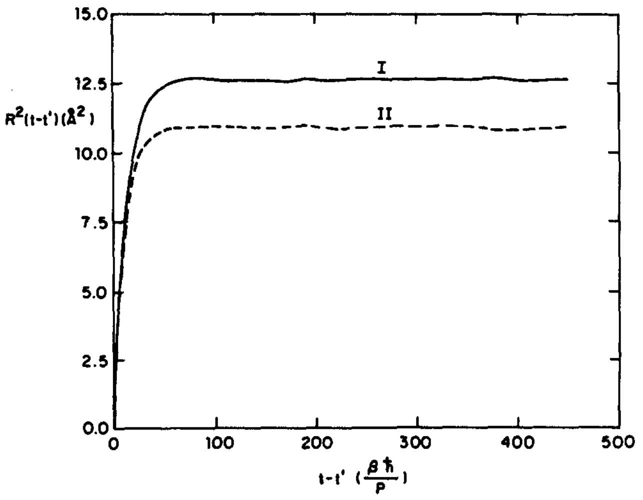

FIG. 8. The imaginary time correlation function $R^2(t-t')$ plotted as a function of $t-t'$ for both model potentials. The initial rapid rise time and the consequent independence of $t-t'$ indicates ground state dominance. The value of R^2 at $\beta\hbar/2$ gives an indication of the size of the electron, with model potential II giving a more compact electron than potential I.

$\langle R\rangle^2$ turns out to be 0.2.

It is also useful to calculate the Euclidian time correlation function $R^2(|t-t'|)$ defined as[48]

$$R^2(|t-t'|) = \langle |r^{(t)} - r^{(t')}|^2\rangle, \tag{24}$$

which expresses the spatial correlations between the beads and consequently the size of the polymer. In Fig. 8, $R^2(\tau)$ is plotted as a function of τ. It is seen that both $R^2_{\rm I}(\tau)$ and $R^2_{\rm II}(\tau)$ rise quickly from zero to their plateau values. This is an indication that the electron is found in the ground state.[48] The value of $[R^2(\beta\hbar/2)]^{1/2}$ obtained using model potential II is about 15% smaller than calculated using potential I. This is, of course, consistent with the cavity radius calculations discussed above. If there is ground state dominance in $R^2(\tau)$, then $R^2(\tau)$ will rise exponentially and the characteristic rise time, τ_c, [a time in which $R^2(\tau)$ reaches the plateau value] can easily be calculated. The mean excitation energy ΔE, which is the average energy difference between the ground state and the lowest excited state of the electron may be obtained as

$$\Delta E = \frac{\hbar}{\tau_c}.$$

This calculation gives $\Delta E = 1.76$ eV for potential I and $\Delta E = 2.07$ eV for potential II. Surprisingly, potential I is in better accord with the experimental result $\Delta E = 1.72$ eV[49] than potential I. It should be emphasized that this is just an estimate and for a proper calculation of the optical absorption spectrum a real dynamic calculation is necessary.[13] Since the ground state dominates, it is interesting to speculate on the nature of this state. The ground state dominance along with the nearly spherical cavity suggests that the electron is in an S state. The broad, featureless, optical absorption spectrum indicates that there are not very many bound states associated with the localized electron. This is also consistent with the shallow well depth predicted by the effective potential. Given a spherical cavity it is likely from optical selection rules that the transition is from $1S \rightarrow 2P$ state.

It is interesting to consider the change in the local water structure induced by the electron. A probe of this would involve calculating the radial distribution functions $g_{\rm OO}(r)$, $g_{\rm OH}(r)$ and $g_{\rm HH}(r)$ by including the water molecules directly affected by the electron. A comparison of these distribution functions with that obtained in the bulk should reveal the influence of the electron in altering the local structure of the water. In obtaining the local pair correlation functions, averages were performed over all pairs of water molecules such that at least one of the molecules in a pair lies within a radial shell. The radial shell was choosen to be within 3.6 Å from the electron center-of-mass. This region contains about four water molecules. The bulk correlation functions were obtained by averaging over all pairs of water molecules such that no solvent molecules lies within the radial shell specified above. It was found that there were negligible differences in the local radial distribution functions between the two model potentials. In what follows, we shall present the results obtained using the second potential energy surface.

In Fig. 9 we plot the local external radial distribution functions $g_{\rm OO}(r)$, $g_{\rm OH}(r)$, and $g_{\rm HH}(r)$ as well as the corre-

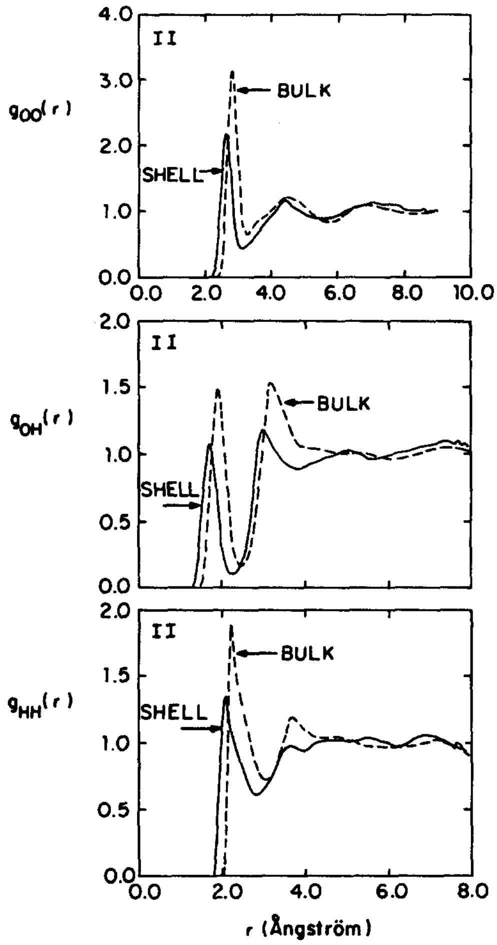

FIG. 9. The shell and bulk radial distribution functions $g_{\rm OO}(r)$, $g_{\rm OH}(r)$, and $g_{\rm HH}(r)$ for model potential II. The shell distribution is calculated using only those pairs of water molecules that have one member inside a radius of 3.5 Å from the electron center-of-mass, whereas the bulk distribution is computed for both molecules outside this distance. Similar graphs for model potential I shows only a negligible difference. All graphs clearly indicate a loss of one hydrogen bond for the molecules inside the shell around the electron cloud. This is seen in the ~25% reduction of the first peak in the distribution.

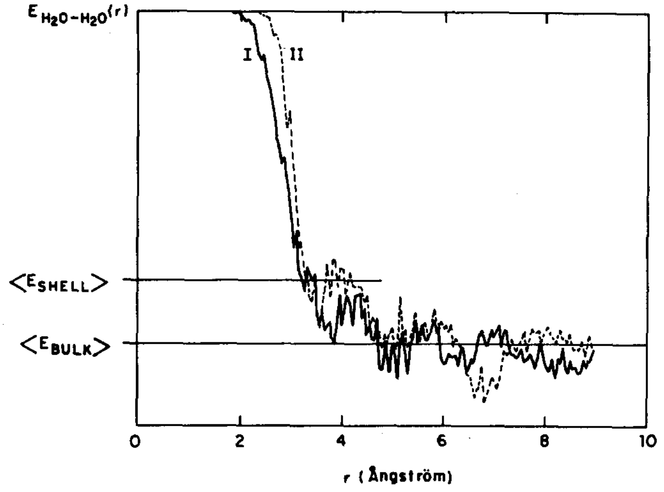

FIG. 10. The solvent–solvent energy calculated as a function of the distance away from the electron barycenter for potentials I and II. The graph shows the energetic loss of the solvent shell molecules due to the loss of a hydrogen bond. See Fig. 2(a) for the corresponding density distribution.

sponding bulk functions $g_{\alpha\beta}(r)$. Figure 10(a), which shows the oxygen–oxygen pair correlation function, clearly indicates a significant decrease in shell oxygen density vs bulk oxygen density. The location of the first peak is shifted in by 0.2 Å and the height of the first peak is reduced almost exactly by 25%. This suggests that the water molecules in the radial shell engage in only three hydrogen bonds as compared to four in the bulk liquid. In the process of accommodating the cavity created by the localized electron, the closest water molecules are pushed back into the liquid. This diminishes the distances between the shell water molecules and its three hydrogen bonded neighbors. This is more clearly seen in Fig. 9(b), which compares the $g_{OH}(r)$ for the shell (shown as a solid curve) and the bulk (shown as a dotted curve). The first peak, corresponding to the hydrogen-bonded water neighbor, is pushed in closer. It is also seen that the two peaks in the shell $g_{OH}(r)$ are about 30% smaller than that of the bulk, indicating a disruption of the local hydrogen bonded structure. The last panel, Fig. 9(c), which compares hydrogen–hydrogen pair correlation function $g_{HH}(r)$ for the shell and the bulk region also indicates the same effect. The hydrogens affected by the presence of the electron are drawn closer together than the hydrogen atoms in the bulk. It is the anticipation of such changes in the local structure due to the excess electron that had caused earlier workers to introduce additional repulsive terms in the potential to account for the proximity of the water molecules closer to the electron. This aspect is rather dramatically borne out in the present work as well. In Fig. 10, radial solvent–solvent energy distributions are given. This is defined as being the total solvent interaction of a water molecule at a distance r from the electron barycenter. This figure demonstrates the difference in the energies of water molecules in the radial shell and that seen in the bulk. The water molecules closer to the cavity have higher energy which is consistent with the proximity of the molecules as indicated by the local structure and the destruction of the hydrogen bonds. This figure also shows a rather sharp transition in the energy between the solvent molecules in the bulk and the shell. A similar graph for potential I (shown in solid) exhibits a rather continuous transition. This may have been anticipated from the rather broad electron center-of-mass oxygen radial distribution function obtained using the first potential energy surface.

B. Energetics of the solvated electron

The solvent–solvent energy for the central force model of water is well documented and thus the question of interest is the extent to which the electron affects the solvent–solvent energy. In addition the electron–solvent energy gives an indication of the strength of interaction between the electron and liquid water. We have already noted (see Fig. 9) that the electron significantly alters the local structure and consequently the interaction energy between the water molecules and the electron. However, on the whole, the influence of the electron is essentially restricted to the first shell of water molecules. In Table I, we present the various potential energy contributions for both model potentials.

In contrast to the difference seen in the structural aspects of the hydrated electron between the two model potentials we note that their energies are comparable. This is understandable because the primary contribution to the electron solvent energy comes from the static potential and to a lesser extent the polarization potential. The latter is dominated by the r^{-4} term and the corrections to this term are higher order in r^{-1}.

The electron does seem to disrupt the local hydrogen bonds, making the water molecules closer to the electron engage in only three hydrogen bonds. This is indicated in Fig. 11 where the hydrogen bond distribution for the shell and the bulk region for the two potentials are shown. This figure clearly shows that the water molecules in the shell

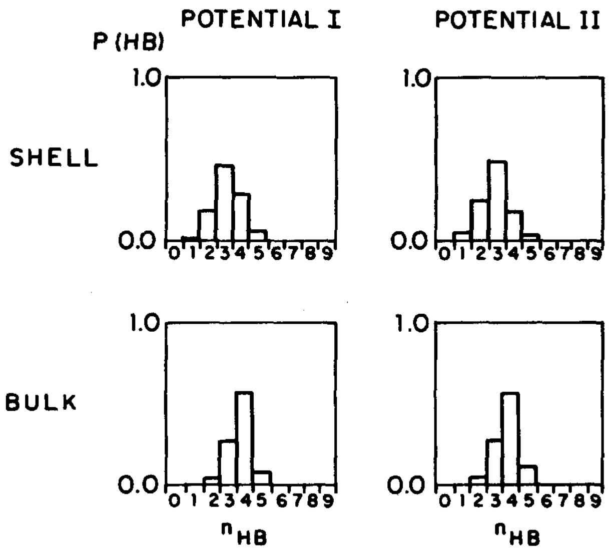

FIG. 11. The hydrogen bond distribution for the shell and the bulk region for the two potentials are shown. A molecule pair is considered to be hydrogen bonded if their potential energy exceeds 4.0 kcal/mol. The shell region shows the hydrogen bond probability to be at a maximum for three hydrogen bonds vs four in the bulk.

engage in three hydrogen bonds. The bulk hydrogen bond distribution is attained at a radial distance of about 3–4 Å from the electron barycenter. This bulk value is attained at a shorter distance for potential I than for potential II. The probability of finding three hydrogen bonds becomes negligible outside the shell with virtually no difference between the model potentials.

V. CONCLUSIONS

This paper is concerned with the detailed analysis of the equilibrium properties of the hydrated electron. We first devised an appropriate electron-water pseudopotential by relying heavily on the so-called effective potential (or optical potential) approach to electron–molecule scattering. This potential was used in path integral Monte Carlo simulations with a sophisticated staging algorithm to calculate various equilibrium correlation functions. These correlation functions provide a very detailed picture of the structure of the hydrated electron. This sort of approach is quite general and can be used to study the behavior of an excess electron in other polar solvents as well.[18–20] The detailed study presented here has led us to the following conclusions:

(i) The electron forms a cavity even if the initial state is delocalized. The radius of the spherical cavity is estimated to be between 2.1–2.3 Å. The fluctuations in the cavity radius is approximated quite well by a Gaussian and the square root of the variance is about 0.1 Å.

(ii) The calculation of the imaginary time correlation function characterizing the bead–bead correlations suggests that the electron is found in the ground state of the water cavity. An estimate of the mean excitation energy compares well with the maximum in the optical absorption spectrum. The ground state dominance along with various other correlation functions allow us to suggest that the ground state is a $1S$ state.

(iii) One of the advantages of the path integral Monte Carlo simulation is that one can probe the response of the solvent molecules to the presence of the excess electron. The study presented here reveals a number of interesting features. We have indicated that there does not appear to be very clear evidence for a sharp shell structure around the electron. This is in agreement with the simulations of Jonah *et al.*[19] and Schnitker and Rossky.[20] The number of water molecules within a distance of 3.6 Å from the electron barycenter is about four. The solvent molecules closest to the electron have their OH bonds pointing towards the electron barycenter. This stands in contrast to the previously advocated dipole oriented model but is in agreement with other recent path integral simulations.[18–20] It should be pointed out that the feature in the potential that induces the OH bond orientation is the static term which describes the interaction potential of the electron with the unperturbed charge density distribution of the water molecule.

(iv) The density of the water molecules around the electron is considerably different from that observed in the bulk. This dramatic difference is most clearly seen by comparing the local solvent radial distribution functions and the corresponding pair correlation functions in the bulk. The solvent–solvent energy in the shell is also considerably higher than that of the bulk water molecules. It was also shown that the average number of hydrogen bonds formed by the water molecules in the shell region is one less than formed by the solvent molecules in the bulk.

(v) In this article, we have used two model potential surfaces to describe the electron–water interaction. The difference in the two potentials arises from the treatment of the polarization effect. In potential II, we explicitly account for the many-body polarization effects by self-consistently treating the induced dipoles on the (polarizable) water molecules in the presence of the electron. We have shown that the inclusion of the self-consistent treatment of the polarization potential has a significant effect on the structural properties leading to a stronger effective repulsion between electron and solvent. This is seen by examining the pair correlation functions $g_{e^-_{\rm com}\text{-O}}(r)$, $g_{e^-_{\rm com}\text{-H}}(r)$ and the orientational correlation function $P_D(\theta)$ and $P_{\rm OH}(\theta)$. On the other hand, there is negligible difference in the solvent–solvent energy. However, the scheme for treating the polarization effects (without resorting to mean-field treatments) in quantum systems presented here is quite general and will prove important in investigating the states of an excess electron in other highly polarizable systems.

(vi) From the technical point of performing path integral Monte Carlo calculations, it is becoming increasingly clear that in order to obtain reliable results one has to resort to quite sophisticated sampling methods. The algorithm suggested by Pollock and Ceperly seems particularly suited for a variety of problems.[41–43] This algorithm and others[50,51] are essential when the number of beads in the electron polymer becomes large. It would be surprising if the primitive algorithm used in either MD or MC simulations gives accurate results.

The path integral method in combination with the effective potential approach seems to be quite reliable in investigating the properties of an excess electron in polar solvents. However, as noted in the Introduction, several problems remain. We are still far away from simulating the dynamical properties of the solvated electron which are needed to compare directly with experiments. In fact, until these calculations are performed, the accuracy of the pseudopotentials devised here and elsewhere cannot be judged. Fortunately, the methodology for performing these real time calculations have been proposed,[52] and thus it is realistic to expect that these simulations will be performed in a few years.

ACKNOWLEDGMENTS

We (B. J. B. and A. W.) wish to thank D. F. Coker for helpful discussions. We thank J. Schnitker and P. Rossky for a careful reading of the manuscript. A. W. also wishes to thank C. Pangali of the Amdahl Corporation for discussions regarding the vectorization of the computer codes and for providing time on the Amdahl 1200 supercomputer under the preliminary feasability studies of the project.

APPENDIX: CONVERGENCE WITH RESPECT TO *P*

The path integral formulation is formally exact only in the limit of $P \to \infty$. In practice, however, P is increased until the relevant physical properties of the system do not change. The convergence of the results was ascertained by studying various properties of the electron with increasing P.

The electron–oxygen pair correlation function, $g_{e^-–O}(r)$, was studied as a function of P. This was deemed to be a sensitive test of the convergence with respect to P. In Fig. 12, we show $g_{e^-–O}(r)$ for model potential I for $P = 90$, 450, and 900. It is absolutely clear from Fig. 12 that as one changes P from 90 to 450 (or 900) the pair correlation function changes. The electron–water interaction is never strong enough to induce any structural changes by a single bead for any P, hence the absolute lack of shell structure. There is a clear difference between $P = 90$ and $P = 450$, 900. This figure allows us to conclude that $P = 900$ is sufficient to ensure convergence of the true electron oxygen pair correlation function.

Another useful criterion of convergence of the results with respect to P is indicated by the change in the interaction potential between a water molecule and the electron over the average distance between two connected beads on the electron chain. For $P = 900$, the average distance between two neighboring beads, $\langle \Delta r^2_{t,t+1} \rangle^{1/2}$, was 1.0 Å as opposed to ~ 2.4 Å for the $P = 90$ case. An estimate of how much the energy changes over an angstrom at typical distances from a water molecule is approximated from Fig. 1 to be about 0.2 eV. Thus for $P = 900$ the change in energy is less than 1% of kT whereas for $P = 90$ the energy difference is $\sim 20\%$ of kT. The energy scale in the problem is set by kT and consequently the corrections to the Trotter formula arising from the higher order terms is expected to be small. This also suggests (does not prove) that $P = 900$ may be adequate.

From the above discussion it is evident that the results obtained with $P = 900$ differs dramatically from those with $P = 90$. In addition, the results obtained using $P = 450$ and $P = 900$ are in good agreement with each other. It is plausible that $P = 900$ represents a converged results, but given the limitations on supercomputer time, we could not carry out simulations with even higher values of P to verify this.

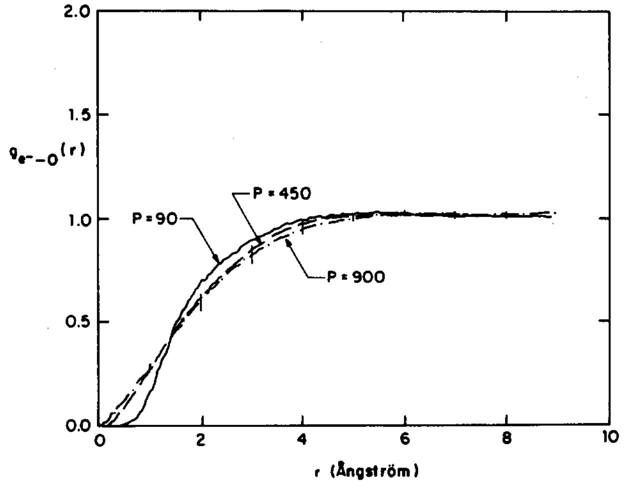

FIG. 12. The true electronic pair correlation function $g_{e^-–O}(r)$ as a function of the number of pseudoparticles used in the simulation employing model potential I. Error bars are indicated for some points on the $P = 900$ graph.

[1]E. J. Hart and M. Anbar, *The Hydrated Electron* (Wiley, New York, 1970).

[2]*Electrons in Fluids*, edited by J. Jortner and N. R. Kestner (Springer, New York, 1973).

[3]*Electron–Solvent and Anion–Solvent Interactions*, edited by L. Kevan and B. C. Webster (Elsevier, New York, 1976).

[4]G. A. Kenney-Wallace, Adv. Chem. Phys. **57**, 535 (1981); G. A. Kenney-Wallace and C. D. Jonah, J. Phys. Chem. **86**, 2572 (1982).

[5]See the chapter by N. R. Kestner in Ref. 3.

[6]For a classification of the excess electron states see J. Jortner and A. Gaathon, Can. J. Chem. **55**, 1801 (1977).

[7]D. A. Copeland, N. R. Kestner, and J. Jortner, J. Chem. Phys. **53**, 1189 (1970).

[8]For an earlier application of this method to electron localization in water clusters see A. Wallqvist, D. Thirumalai, and B. J. Berne, J. Chem. Phys. **85**, 1583 (1986).

[9]E. J. Hart, in *Radiation Chemistry of Aqueous Systems*, edited by G. Stein (Interscience, New York, 1968), p. 73; U. Schindewolf, H. Kohrmann, and G. Lang, Angew. Chem. Int. Ed. Engl. **8**, 512 (1969).

[10]For a summary see G. A. Kenney-Wallace, Acc. Chem. Res. **11**, 433 (1978).

[11]R. R. Hentz, Farhataziz, and E. M. Hansen, J. Chem. Phys. **55**, 4974 (1972).

[12]R. R. Hentz, Farhataziz, and E. M. Hansen, J. Chem. Phys. **57**, 2959 (1974).

[13]D. Thirumalai and B. J. Berne, Chem. Phys. Lett. **116**, 471 (1985); R. D. Coalson, J. Chem. Phys. **83**, 688 (1985).

[14]S. Schlik, P. A. Narayana, and L. Kevan, J. Chem. Phys. **64**, 3153 (1976).

[15]D. F. Feng and L. Kevan, Chem. Rev. **80**, 1 (1980).

[16]L. Kevan, J. Phys. Chem. **85**, 1628 (1981).

[17]D. P. Lin and L. Kevan, J. Phys. Chem. **86**, 2629 (1982).

[18]M. Sprik, R. W. Impey, and M. L. Klein, J. Chem. Phys. **83**, 5802 (1985); J. Stat. Phys. **43**, 967 (1986).

[19]C. D. Jonah, C. Romero, and A. Rahman, Chem. Phys. Lett. **123**, 209 (1986).

[20]P. J. Rossky, J. Schnitker, and R. A. Kuharski, J. Stat. Phys. **43**, 949 (1986); J. Schnitker and P. Rossky, J. Chem. Phys. (in press, 1986).

[21]M. Newton, J. Phys. Chem. **79**, 2795 (1975).

[22]H. L. Lemberg and F. H. Stillinger, J. Chem. Phys. **62**, 1677 (1975); A. Rahman, F. H. Stillinger, and H. L. Lemberg, J. Chem. Phys. **63**, 5223 (1975).

[23]J. R. Reimers and R. O. Watts, Chem. Phys. Lett. **94**, 222 (1982); Chem. Phys. **85**, 83 (1984); Mol. Phys. **52**, 357 (1984). Note that in these papers the dimensionless coordinate S_3 is everywhere erroneously defined as being twice as large as it should be.

[24]D. Thirumalai, A. Wallqvist, and B. J. Berne, J. Stat. Phys. **43**, 973 (1986).

[25]C. H. Douglass, D. A. Weil, P. A. Chartier, R. A. Eades, D. G. Truhlar, and D. A. Dixon in *Chemical Applications of Atomic and Molecular Electrostatic Potentials*, edited by P. Politzer and D. G. Truhlar (Plenum, New York, 1981).

[26]N. F. Lane, Rev. Mod. Phys. **52**, 29 (1980).

[27]D. G. Truhlar, in *Chemical Applications of Atomic and Molecular Electrostatic Potentials*, edited by P. Politzer and D. G. Truhlar (Plenum, New York, 1981); D. Thirumalai, University of Minnesota, Ph.D. thesis, 1982 (unpublished).

[28]J. C. Slater, in *Advances in Quantum Chemistry*, edited by P.-O. Löwdin (Academic, New York, 1972), Vol. 6.

[29]See for example, M. E. Riley and D. G. Truhlar, J. Chem. Phys. **63**, 2182 (1975), and references therein.

[30]For a recent discussion of the various forms of the switching function and their effect on electron–molecule scattering, see A. Jain and D. G. Thompson, J. Phys. B **15**, 1631 (1982).

[31]P. G. Burke and N. Chandra, J. Phys. B **5**, 1696 (1972).

[32]D. G. Truhlar, D. A. Dixon, and R. A. Eades in *Electron–Molecule and Photon–Molecule Collisions*, edited by T. N. Resigno, V. McKoy, and B. Schneider (Plenum, New York, 1979).

[33]The use of one-center expansion was tested extensively for obtaining the ground state energy of molecules by R. Moccia, J. Chem. Phys. **40**, 2164 (1964).

[34]F. A. Gianturco and D. G. Thompson, Chem. Phys. **14**, 111 (1976). These authors compared the results of the calculation of static potential for AH_n molecules obtained using both the one center expansion of the wave function and the multicenter wave functions.

[35]D. Thirumalai (unpublished results).

[36]F. H. Stillinger and C. W. David, J. Chem. Phys. **69**, 1473 (1978).
[37]D. Chandler and P. G. Wolynes, J. Chem. Phys. **74**, 4078 (1981).
[38]A pass involves moving each bead on the ring once. A pseudoparticle making a large excursion in one pass is likely to be pulled back into the backbone of the isomorphic pseudoparticle chain in a subsequent pass.
[39]D. E. Rouse, J. Chem. Phys. **21**, 1272 (1953).
[40]M. F. Herman, E. J. Bruskin, and B. J. Berne, J. Chem. Phys. **78**, 4103 (1982); D. Thirumalai; E. J. Bruskin, and B. J. Berne, J. Chem. Phys. **79**, 5063 (1983); J. Bartholomew, R. Hall, and B. J. Berne, Phys. Rev. B **32**, 548 (1985); M. Parrinello and A. Rahman, J. Chem. Phys. **80**, 860 (1984).
[41]E. L. Pollock and D. M. Ceperly, Phys. Rev. B **30**, 2555 (1984).
[42]L. D. Fosdick and H. F. Jordan, Phys. Rev. **143**, 58 (1965); H. F. Jordan and L.D. Fosdick, Phys. Rev. **171**, 128 (1967).
[43]D. Coker, B. J. Berne, and D. Thirumalai, J. Chem. Phys. **86**, 5689 (1987).
[44]A. Wallqvist, B. J. Berne, and C. Pangali, Computer (in press, 1986).
[45]R. W. Impey, P. A. Madden, and I. R. McDonald, J. Phys. Chem. **87**, 5071 (1983).
[46]M. Mezei and D. L. Beveridge, J. Chem. Phys. **74**, 6092 (1981).
[47]A. Gaathon and J. Jortner, in Ref. 2, p. 429.
[48]D. Chandler, Y. Singh, and D. M. Richardson, J. Chem. Phys. **81**, 1975 (1981).
[49]See for example, F. Y. You and G. R. Freeman, Can. J. Chem. **60**, 1809 (1982).
[50]M. Sprik, M. L. Klein, and D. Chandler, Phys. Rev. B **31**, 4234 (1985); **32**, 545 (1985); J. Chem. Phys. **83**, 3202 (1985).
[51]J. D. Doll, R. D. Coalson, and D. L. Freeman, Phys. Rev. Lett. **55**, 1 (1985).
[52]For a review, see B. J. Berne and D. Thirumalai, Ann. Rev. Phys. Chem. **37**, 401 (1986).